


TECHNICAL SPOTLIGHT

TECHNICAL SPOTLIGHT

Super-resolution structural analysis of dendritic spines using three-dimensional structured illumination microscopy in cleared mouse brain slices

Kazuaki Sawada,^{1,2}  Ryosuke Kawakami,^{1,2} Ryuichi Shigemoto³ and Tomomi Nemoto^{1,2,4}¹Graduate School of Information Science and Technology, Hokkaido University, Sapporo, Japan²Research Institute for Electronic Science, Hokkaido University, Sapporo, Hokkaido, Japan³Institute of Science and Technology Austria, Klosterneuburg, Austria⁴Laboratory of Molecular and Cellular Biophysics, Research Institute for Electronic Science, Hokkaido University, Kita 20, Nishi 10, Kita, Sapporo 001-0020, Hokkaido, Japan

Keywords: dendritic spines, fixed mouse brain, prefrontal cortex, three-dimensional structured illumination microscopy, tissue clearing methods

Abstract

Three-dimensional (3D) super-resolution microscopy technique structured illumination microscopy (SIM) imaging of dendritic spines along the dendrite has not been previously performed in fixed tissues, mainly due to deterioration of the stripe pattern of the excitation laser induced by light scattering and optical aberrations. To address this issue and solve these optical problems, we applied a novel clearing reagent, LUCID, to fixed brains. In SIM imaging, the penetration depth and the spatial resolution were improved in LUCID-treated slices, and 160-nm spatial resolution was obtained in a large portion of the imaging volume on a single apical dendrite. Furthermore, in a morphological analysis of spine heads of layer V pyramidal neurons (L5PNs) in the medial prefrontal cortex (mPFC) of chronic dexamethasone (Dex)-treated mice, SIM imaging revealed an altered distribution of spine forms that could not be detected by high-NA confocal imaging. Thus, super-resolution SIM imaging represents a promising high-throughput method for revealing spine morphologies in single dendrites.

Introduction

Microscopy, including electron microscopy (EM) and optical microscopy, is widely employed for biological research. EM has revealed the fine structure of neurons, including excitatory synapses on dendritic spines, with spatial resolution of a few nanometers (Arellano *et al.*, 2007). Each individual neuron bears a huge number of dendritic spines, which constitute the site where input is received (Collin *et al.*, 1997; Harris & Shepherd, 2015; Shigematsu *et al.*, 2016). Recent studies of synaptic plasticity have revealed a correlation between forms of spine heads and synapse transmission efficiency

(Nusser *et al.*, 1998; Matsuzaki *et al.*, 2001; Tønnesen *et al.*, 2014). To elucidate the function of dendritic spines in synaptic plasticity, it is necessary to perform mass analysis of spine morphologies in an intact whole neuron. With EM, however, acquisition of images and analysis of spine morphologies along a single neuron requires too much effort to be practical. On the other hand, an optical microscopy can visualize neuronal structures along a single neuron (Kasthuri & Lichtman, 2003; Livet *et al.*, 2007; Lichtman *et al.*, 2008), and relatively simple optical methods have revealed several properties of synapses. However, optical microscopy cannot clearly observe the fine forms of dendritic spines because the diffraction limit of classical optical microscopy techniques (~200 nm; Conchello *et al.*, 1994) is larger than the thin type of spines (~100 nm; Arellano *et al.*, 2007). To overcome this limitation, super-resolution fluorescence microscopes have been developed and applied to morphological analyses, including elucidation of entire spine forms and localization of synaptic proteins (Urban *et al.*, 2011; Lakadamyali *et al.*, 2012; Tønnesen & Nägerl, 2013).

The super-resolution microscopy technique structured illumination microscopy (SIM; Neil *et al.*, 1997; Gustafsson, 2000) can obtain three-dimensional (3D) images at a spatial resolution of about 115 nm

Correspondence: Prof Tomomi Nemoto, ²Laboratory of Molecular and Cellular Biophysics, as above. E-mail: tn@es.hokudai.ac.jp

Received 17 May 2017, revised 21 February 2018, accepted 1 March 2018

Edited by Ania Majewska. Reviewed by Valentin Nägerl, University of Bordeaux, France; Harold MacGillavry, Utrecht University, Netherlands; Jan Tønnesen, Achucarro Basque Center for Neuroscience, Spain

All peer review communications can be found with the online version of the article.

[The copyright line for this article was changed on 11 April, 2018, after original online publication]

(theoretically, at 488 nm excitation). SIM employs stripe patterns in the excitation laser that yield Moiré pattern images, which are essential for computing the high-frequency component. SIM imaging is technically straightforward and can be easily applied to typical samples of interest to biological researchers. Hence, we applied SIM imaging in fixed brains to perform morphological analysis along single dendrites.

However, SIM imaging in fixed brain slices could not achieve super-resolution in deep regions, largely due to serious deterioration of the stripe pattern (Kim & Wilson, 2011). This deterioration was probably caused by a reduction in laser power or by a degradation of focus. The power of the excitation laser was reduced at the focal point due to light scattering. Thus, the specific stripe pattern could not penetrate to deeper regions of fixed brain. To reduce the effects of such light scattering, several clearing methods (Hama *et al.*, 2011, 2015; Aoyagi *et al.*, 2015; Richardson & Lichtman, 2015; Ke *et al.*, 2016) for fixed brains have been developed over the past few years. On the other hand, the focal properties deteriorated due to wavefront aberrations (Gibson & Lanni, 1991; Sheppard *et al.*, 1994; Booth *et al.*, 1998). In particular, the spherical aberration, which is usually induced by a difference in refractive index (RI) between the sample and immersion medium, significantly degrades focus. This degradation of focal properties induces the deterioration of the stripe pattern of the excitation laser and thus decreases the spatial resolution. Another effect of the difference in the RI is that the index mismatch between the sample and the cover glass degrades the spatial resolution by inducing total reflection at the edge of the excitation light, thereby decreasing the performance of a high numerical aperture (NA) objective (Axelrod, 2001). To decrease the index mismatch, the RI of specimens must be adjusted to that of the immersion liquid of the objective lens. In a previous report, to adjust the RI of fixed brains, we applied the 2,2'-thio-diethanol (TDE)-clearing method (Aoyagi *et al.*, 2015). In addition, adjustment of RI in fixed brains enabled us to perform high-NA confocal imaging of hippocampal neurons.

In this study, we combined a novel clearing method with SIM to conduct super-resolution imaging of dendritic spines along single neurons. As the clearing reagent, we chose the LUCID-A solution (LUCID) based on the TDE (Onodera, 2014; Mizutani *et al.*, 2018), which is an easy and a simple clearing method. Then, we characterized the effects of LUCID in fixed brains. Next, we showed that SIM could visualize the fine forms of dendritic spines in single apical dendrites of LUCID-treated slices. Finally, we performed morphological analyses of spine heads and tried to determine the distribution of forms of spine heads in the mPFC of chronic Dex-treated mice (Cerqueira *et al.*, 2007; Banasr *et al.*, 2011; Duman & Duman, 2015).

Materials and methods

Animals

Female Thy1-EYFP-H transgenic mice (H-line) were bred at Hokkaido University and used for visualizing L5PNs of mPFC ($n = 14$, average 18.8 g). For evaluating effects of clearing reagents, brain slices of H-line mice were used for obtaining representative fluorescence and electron microscopy images of cleared slices ($n = 3$). To evaluate the effects of chronic Dex treatment, H-line mice (8–10 weeks old) were pretreated with dexamethasone (5 mg/kg *i.p.*, Kyoritsu Seiyaku, Tokyo, Japan) or saline (10 mL/kg, *i.p.*, Otsuka Pharmaceutical, Tokyo, Japan) for 21 days at their home cage ($n = 5–6$ per group). Female C57BL/6 mice (Charles River Laboratories, Kingston, NY, USA; $n = 4$, average 20.1 g) were used for evaluating transmission of excitation and fluorescence wavelengths

in cleared slices ($n = 3$) and embedding of 100-nm yellow-green (YG) beads ($n = 3$). All mice were housed with food and water *ad libitum* on a 12 : 12 light–dark cycle (lights on from 08:00 to 20:00), with controlled temperature and humidity. They were housed in conventional room (four mice per cage). The study was carried out under the Guidelines for the Care and Use of Laboratory Animals of the Animal Research Committee of Hokkaido University. All protocols were approved by the Institutional Animal Care and Use Committee of National University Corporation Hokkaido University (Permit Number: 14-0127).

Preparation of cleared fixed brain slices

To fix and preserve EYFP as much as possible, mice were perfused transcardially with fixative containing 4% paraformaldehyde and 0.1% glutaraldehyde in phosphate buffer saline under deep pentobarbital anesthesia (15 mg/kg; *i.p.*). Fixed brains were removed and sliced into 150- or 400- μm sections using a vibratome (7000smz, Campden Instruments, Loughborough, UK). These 150- μm sections were used to observe neurons, and the 400- μm sections were used to evaluate clearing efficiency. In the LUCID-clearing method, brain slices were incubated in the No. 1 solution of LUCID#2 (Nikon, Tokyo, Japan) for 3 h and then placed in the No. 2 solution of LUCID#2 for 3 h. We abbreviated LUCID#2 solution as 'LUCID' in this study. In the TDE60% method, brain slices were placed in TDE60% solution (TDE : PBS = 60 : 40, Sigma-Aldrich, St. Louis, MO, USA) for 6 h.

Measurement of RI and transmittance spectrum

The refractive indices of LUCID and TDE60% were measured with a pocket refractometer (PAL-RI, Atago, Tokyo, Japan). To examine the transmittance spectrum at visible wavelengths, the cortex region was trimmed from each brain slice (thickness, 400 μm) of C57BL/6 mice and recorded using a UV/visible/near-infrared (NIR) spectrophotometer (U-2900, Hitachi, Tokyo, Japan).

Acquisition of wide-field images

To evaluate the state of a transparency, brain slices (thickness, 400 μm) were imaged by transmission microscopy (SZ61/SZ2-ILST, Olympus, Tokyo, Japan) with a camera (DP21, Olympus). Fluorescence images of brain slices (thickness, 150 or 400 μm) of H-line mice were obtained by fluorescence microscopy (IX-70, Olympus) using the indicated objective (Uplan FLN 10 \times NA = 0.30 for local images or Uplan FLN 4 \times NA = 0.13 for large images; Olympus) and filter (YFP-2427A, Semrock, New York, NY, USA).

Transmission electron microscopy

To investigate the effects of a LUCID or TDE60% treatment on fine structures, cleared slices were treated in 1% osmium tetroxide in 0.1 mM PB, dehydrated and then flat-embedded in Durcupan resin (ACM; Fluka, Buchs, Switzerland). Corresponding small parts (0.5–1.0 mm) of the cortex and the striatum area were trimmed; 70-nm-thick sections were collected on Pioloform-coated single-slot grids, contrasted with uranyl acetate and lead citrate and examined with a Tecnai 12 electron microscope (FEI, Hillsboro, OR).

Acquisition of confocal and SIM images

To obtain projection-type images in confocal microscopy or SIM, slices were placed on a glass-bottom dish (No. 1S, Matsunami,

Osaka, Japan). The correction collar of the objectives was adjusted at each imaging to collect spherical aberrations, depending on the depth of the focal point. Images of fluorescence beads were obtained at depths of 0, 10, 20, 40 and 60 μm from the surface of brain slices. Apical dendrites were observed at a depth of 40 μm from the surface.

Confocal images were obtained using a confocal microscope (A1R, Nikon) with a 60 \times oil-immersion lens (NA 1.49). An imaging was acquired two times averaging with area of 42.3 \times 42.3 μm (1024 \times 1024 pixels, 0.041 μm /pixels). A pinhole size of 0.8 A.U. (Nis-Elements AR) was selected because imaging at a smaller pinhole size resulted in photobleaching, preventing visualization of dendritic spines. Image stacks of optical sections were acquired with 0.2- μm Z-steps. In Fig. 2, the laser line at 488 nm was used for excitation, which was the same wavelength used for SIM. In Figs 4 and 5, the laser line at 514 nm was used because it was the most suitable wavelength for exciting EYFP fluorescence. Fluorescence signals at wavelengths of 500–550 nm were detected using a photomultiplier tube. All images were displayed by Nis-Elements AR (ver. 4.13).

Raw SIM images were obtained using a Nikon N-SIM through a 100 \times oil-immersion objective (Nikon CFI Apo TIRF 100xH for a TIRF imaging, NA 1.49). The laser line at 488 nm in a sinusoidal striped pattern was used as excitation light for imaging of EYFPs and 100 nm YG beads. An imaging was acquired with area of 32.6 \times 32.6 μm (16 bit, 1024 \times 1024 pixels, 0.032 μm /pixels). Image stacks of optical sections were acquired with 0.12- μm Z-steps. To demonstrate the existence of the stripe pattern in frequency space, raw SIM images were transformed by fast Fourier transformation (FFT) using the Fiji. Raw images were reconstructed by 3D reconstruct mode in Nis-elements (ver. 4.13).

Measurement of FWHMs embedded 100-nm YG beads in the brain

To evaluate focusing property in fixed brain slices, C57BL/6 mice were injected in a mPFC region with 1% 100-nm YG bead solution in PBS (4 μL , Invitrogen, CA, USA) using a microinjector (oil pressure) and perfused with fixative solutions after 2–3 h. FWHMs in the image of fluorescent beads ($n = 10$, each at Figs 2 and 3g and h; $n = 20$, each at measurements of spatial resolution in SIM imaging) were calculated by fitted gauss curve (Origin Pro 9.0J) to line profile across the point of maximum intensity of the spine (Fiji).

Morphological analysis of spine forms

We represented spine forms as the elliptical form because the typical classification (Yuste & Bonhoeffer, 2004; Fig. S1a) was not suitable for morphological analysis of SIM images, as mentioned above. Classically, forms of dendritic spines are divided into four groups: stubby, mushroom, thin and filopodia. The stubby and mushroom types, in contrast to the thin and filopodia types, were stable and have larger spine heads, and thus larger numbers of postsynaptic receptors. However, due to the diversity spine forms, these typical classifications were not suitable for morphological analysis in the cerebral cortex. On the other hands, spine sizes were also considered as an object of analysis and were represented by volume and the fluorescence intensity. However, these representations were not suitable for SIM images, because fluorescence intensities of SIM images were obtained by computation and had large axial FWHMs. Therefore, we represented spine forms as the elliptical form to distinguish whether the spine forms were of the stubby and mushroom type.

In the analysis of spine forms, we selected spines on the apical dendrites on L5PNs from the distance of 20 μm at cortex layers II/III region in confocal images (control group, $n = 115$, 2 mice; chronic Dex-treated group, $n = 221$, 3 mice) and SIM images (control group, $n = 273$, 3 mice; chronic Dex-treated group, $n = 259$, 3 mice). The filopodia types of dendritic spines and axons were distinguished based on their lengths. To represent elliptical forms of dendritic spines, FWHMs were calculated from the fitted gauss curve to fluorescence intensities in the major and a minor axis, which were obtained by line acquisition (Nis-Elements ver. 4.13) in the maximum-intensity projection image of dendritic spines. The major axis was determined based on the appearance of the image, and the minor axis was then defined as perpendicular to the major axis.

Data analysis

All groups were tested for normality by the Shapiro–Wilk test. The spine heads dataset had a non-normal distribution, but the other data sets were normally distributed. The Mann–Whitney *U*-test was used for comparisons of non-normal distribution.

Results

Improvement of focal properties in LUCID-treated slices

We first examined the clearing effects of LUCID in fixed brain slices. LUCID treatment cleared brain slices (thickness, 400 μm) within 6 h, similar to the rapid effects of TDE60% (Aoyagi *et al.*, 2015; Fig. 1a). To evaluate the transparency of brain slices, we compared transmission and fluorescence images between LUCID- and TDE60%-treated slices from Thy1-EYFP-H transgenic mice (H-line; Feng *et al.*, 2000). In transmission images, white light was transmitted as efficiently through LUCID-treated slices as through TDE60%-treated slices (Fig. 1a). In fluorescence images, cell bodies and their apical dendrites of neurons could be clearly observed in both types of cleared slices, whereas EYFP fluorescence signals became blurry in non-treated slices (Fig. 1b and c). Thus, both types of clearing treatments decreased the background noise of EYFP fluorescence. Fluorescence signals were almost completely preserved by immersion in LUCID (data not shown) or low-concentration TDE solutions, whereas a high concentration of TDE solution quenches fluorescent proteins (Aoyagi *et al.*, 2015). Next, we examined the transmittance spectrum in cortical regions to evaluate the transmission of excitation and fluorescence wavelengths. Much higher transmittance was obtained in cleared slices in comparison with non-treated slices (Fig. 1d). In particular, at the EYFP excitation wavelength of 488 nm, the transmittances of LUCID-, TDE60%- and non-treated slices were 63.25 ± 0.37 , 49.45 ± 1.30 and $0.95 \pm 0.07\%$ (means \pm SEM; $n = 5$ brain slices), respectively. Similarly, transmittances at 527 nm, the spectral maximum of EYFP, were 67.51 ± 0.25 , 54.25 ± 1.28 and $0.98 \pm 0.06\%$, respectively. Therefore, LUCID treatment was more suitable for fluorescence imaging in visible wavelengths than TDE60% treatment.

Because the amphipathic properties of TDE might remove lipids, including those constituting the plasma membrane, we next investigated whether LUCID maintains membrane structures. To evaluate the effects on ultrastructure in fixed brains, cleared slices were restored by washing with phosphate buffer, and then imaged by the EM. In LUCID- and TDE60%-treated slices, continuous membrane structures and synaptic vesicles were observed near characteristic electron-dense regions corresponding to postsynaptic densities in excitatory synapses (Fig. 1e). Thus, membrane and ultrastructure

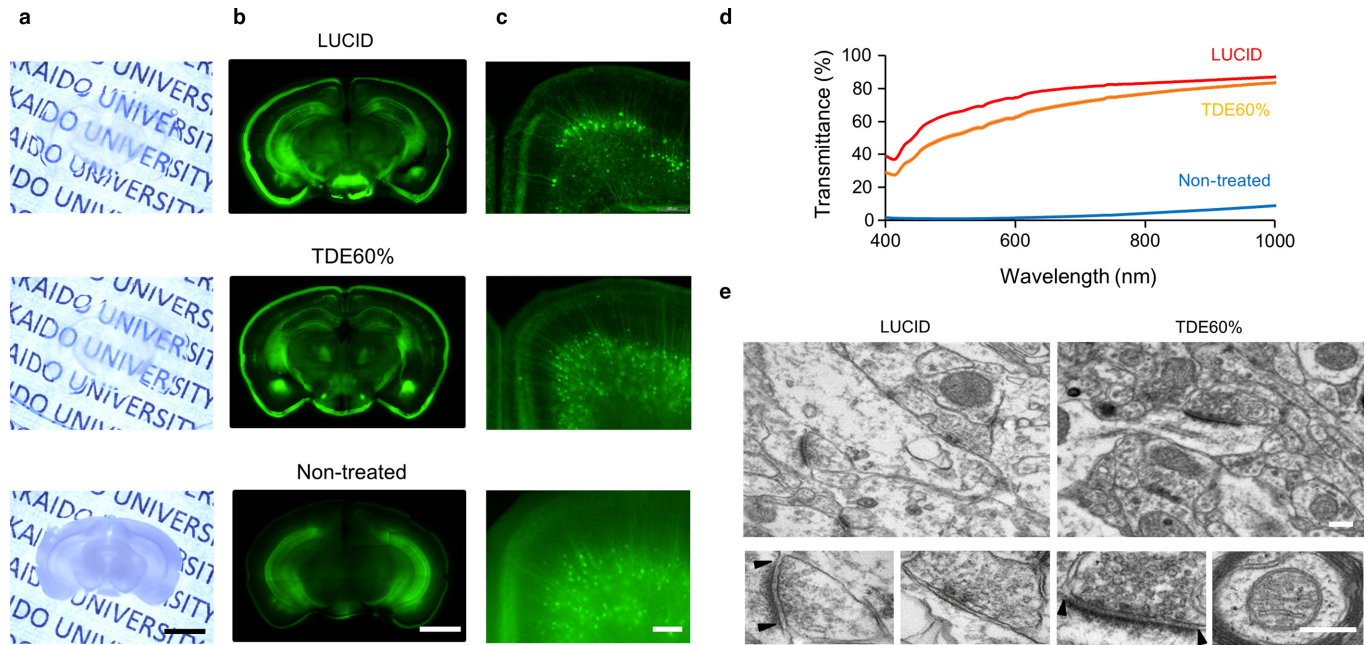


FIG. 1. LUCID decreases light scattering in fixed brains without any destruction of membrane structures. (a–c) Fixed brain slices prepared from Thy1-EYFP-H mice (H-line) after 6-h treatment with LUCID (above), 2,2'-thiodiethanol (TDE) 60% (middle), or PBS (non-treated, above). Light transmission image (a); EYFP fluorescence images (b, c). Thicknesses of brain slices (H-line) were 400 μm (a, b) and 150 μm (c). Scale bars, 2 mm (a, b) and 200 μm (c). (d) Transmission curves of visible wavelengths in the cerebral cortex (thickness, 400 μm ; $n = 5$ each) treated with LUCID (red), TDE60% (yellow), or PBS (blue). Thick lines include SEM. (e) Representative transmission electron microscopy images in the cortex region of LUCID- and TDE60%-treated slices. Magnified images are shown at the bottom. Arrowheads indicate postsynaptic densities. Scale bars, 200 nm. [Colour figure can be viewed at wileyonlinelibrary.com].

were substantially preserved, and the subcellular organelles in the neurons could be observed contiguously. These structures were preserved in the cortex and striatum of the cleared slices (Figs 1e and S2). This result indicated that both clearing treatments caused almost no destruction of membrane structures in fixed brains, similar to results obtained with the ScaleS method (Hama *et al.*, 2015).

We then examined the effects of LUCID treatment in the high-NA confocal imaging method proposed in our previous report (Ke *et al.*, 2016). In LUCID, the RI was 1.496, and did not change significantly as a function of ambient temperature (data not shown). To investigate the focal properties of the excitation laser in brain slices, we obtained fluorescence images from LUCID-, TDE60%- and non-treated slices of H-line mice by confocal microscopy using an oil-immersion objective (NA 1.49). In these confocal images, the fine structures of dendrites were clearly observed at a depth of 10 μm from the slice surface in both types of cleared slices, and less clearly in non-treated slices (Fig. 2a). In addition, dendritic spines in the axial direction were clearly observed in cleared slices, but not in non-treated slices. To evaluate the spatial resolution in these brain slices, we measured full width at the half maximum (FWHM) of 100-nm YG beads embedded in the brain (Cox & Sheppard, 2004). In cleared slices, the beads could be visualized from the surface to a depth of about 60 μm , whereas in non-treated slices, no obvious images could be acquired at depths greater than 10 μm (Fig. 2b). In images of fluorescent beads at a depth of 10 μm , lateral FWHMs on XY images of the focal plane in the LUCID-, TDE60%- and non-treated slices were 201 ± 7 , 192 ± 5 and 223 ± 9 nm (means \pm SEM; $n = 10$ fluorescent beads), respectively, and axial FWHMs in these slices were 731 ± 13 , 589 ± 45 and 701 ± 46 nm, respectively (Fig. 2c). Notably, lateral FWHMs in cleared slices were smaller than those in non-treated slices. In particular, FWHMs at a depth of 40 μm did not increase in either lateral or axial resolution

(Fig. 2d and e). In both types of cleared slices, the axial FWHM increased sharply at depths above 60 and 80 μm in TDE60%- and LUCID-treated slices, respectively. This increase in FWHMs was probably caused by spherical aberrations those were not compensated by a correction collar in the objective lens (Fig. 2e). These results indicated that LUCID treatment might induce high transparency and the penetration depth in confocal images. Furthermore, this treatment improved focal properties in fixed brains and increased the spatial resolution.

SIM imaging of a single dendrite in LUCID-treated slices

LUCID treatment reduced the deterioration of focal properties in fixed brains. Therefore, we hypothesized that the sinusoidal striped excitation light of SIM would be preserved in deep regions of fixed brains treated with LUCID. Hence, we applied LUCID treatment to SIM imaging and tried to acquire super-resolution images of the apical dendrites of L5PNs in H-line mice. In raw images from non-treated slices, we could not observe the sinusoidal striped patterns of fluorescence at a depth of 10 μm . On the other hand, the striped patterns were still sharp and detectable sharply at multiple greater depths in LUCID-treated slices. Furthermore, the characteristic pattern that indicated specific spatial frequencies appeared in a diagonal direction in the fast Fourier Transformation (FFT) image computed from raw images of cleared slices (Fig. 3a and b). On the other hand, the image reconstructed from raw images of non-treated slices contained some artifacts, such as dotted neuronal structures or artificial double images of dendrites in the axial direction (Fig. 3c and d). To evaluate the spatial resolution in SIM images, 100 nm YG beads embedded in the brain were visualized in LUCID-treated slices (Fig. 3e and f). At a depth of 10 μm , lateral and axial FWHMs were 163 ± 1 and 583 ± 4 nm (means \pm SEM; $n = 20$

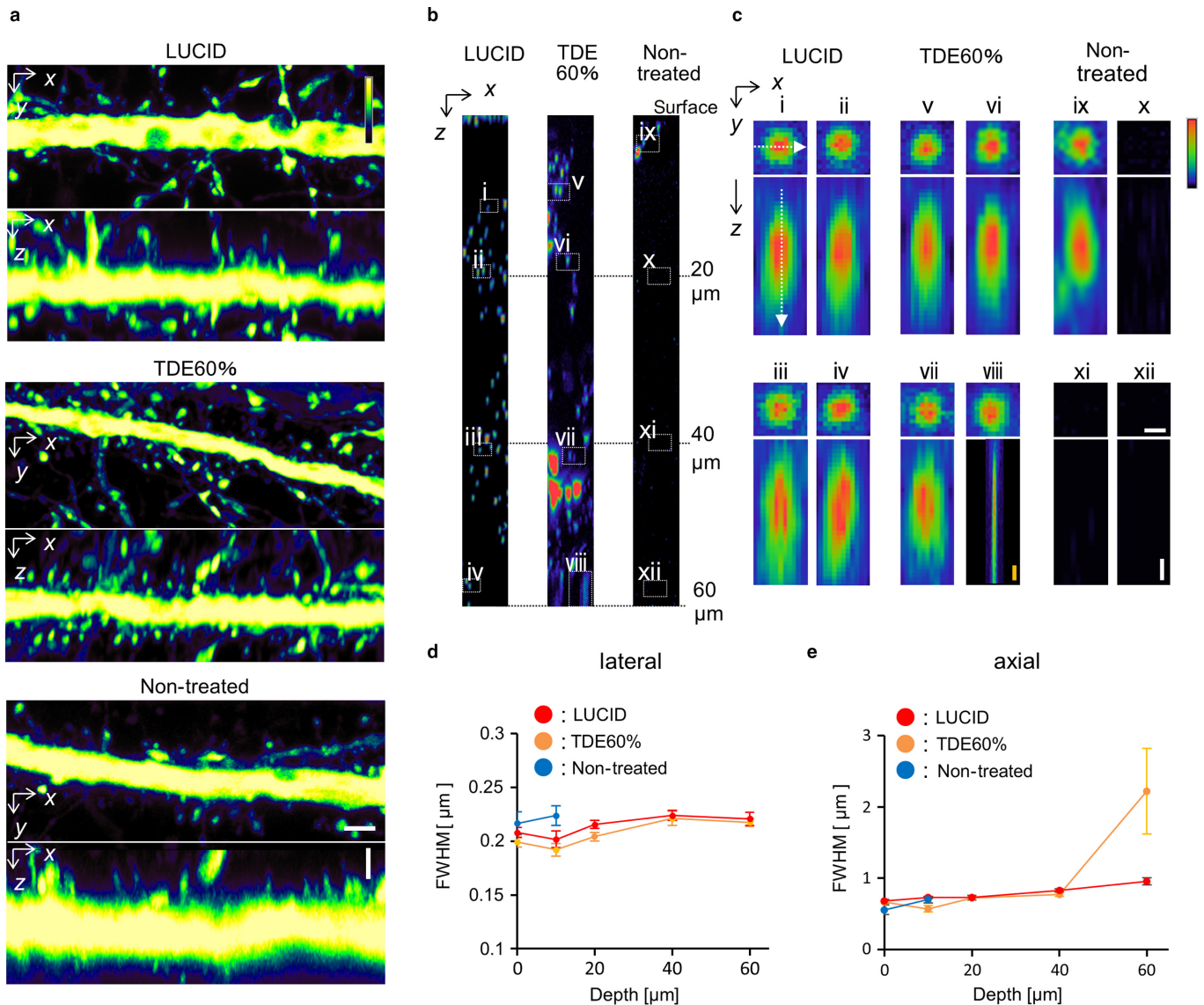


FIG. 2. LUCID and TDE60% treatments improve spatial resolution in confocal images of fixed brains. (a) Representative apical dendrites of layer V pyramidal neurons (L5PNs) in confocal images of LUCID- (above), TDE60%- (middle), and non- (bottom) treated slices of Thy1-EYFP-H mice. Vertical bar indicates the color code. Scale bars, 2 μm . (b, c) Embedded 100-nm yellow-green (YG) beads in brain slices. XZ images of the Z-stack (b). Magnified images of YG beads in regions i–xi are shown in XY and XZ images (c). Dashed lines show how fluorescence intensities were acquired along XY and XZ images. White scale bars indicate 200 nm. Yellow scale bar indicates 1 μm in the axial image of panel viii only. (d, e) Full width at half maximum (FWHM) of 100 nm YG beads ($n = 10$ each) at each depth: lateral FWHMs in XY images (d) and axial FWHMs in XZ images (e) in individual brain slices. All figures were maximum-intensity projection images. [Colour figure can be viewed at wileyonlinelibrary.com].

fluorescence beads) in LUCID-treated slices, whereas those in non-treated slices were 199 ± 7 and 880 ± 30 nm (Fig. S3a), respectively. The lateral FWHM in LUCID-treated samples was below the diffraction limit of classical fluorescence microscopies; thus, we achieved super-resolution imaging in fixed brains. At depths from 10 to 60 μm , this super-resolution using the correcting collar of the objective lens was maintained in lateral images (Fig. 3g), and axial FWHMs of about 580 nm were maintained (Fig. 3h). In addition, the range of depths at which spatial resolution was maintained was altered by the correcting collar (Fig. S3b and c). These results indicated that super-resolution imaging in LUCID-treated slices might be possible within a depth of 60 μm .

Next, we investigated how much volume it was possible to outline in a single neuron using SIM. To this end, we observed single neurons of L5PNs on the mPFC along the main shaft of an apical

dendrite. Fine structures, including dendritic spines, were visualized in a broad area of the cortex from layer V to layer I (distance, ~ 180 μm), similar to the results of high-NA confocal imaging in TDE60%-treated slices (Aoyagi *et al.*, 2015; Fig. 4a and b). We next analyzed forms of spine heads in SIM and confocal images (100 spines each) to determine whether super-resolution imaging could visualize finer dendritic spines than high-NA confocal imaging. For the morphological analysis, we represented spine heads as the lengths of the major and minor axes in a maximum-intensity projection image. In the histogram of the major axis, 42% of dendritic spines within 300 nm were detected in SIM images, whereas only 5% of spines were observed in the high-NA confocal images (Fig. 4c and d). Moreover, in the histogram of the minor axis, 28% of dendritic spines were present within 200 nm in SIM images, whereas no such spines appeared in high-NA confocal images

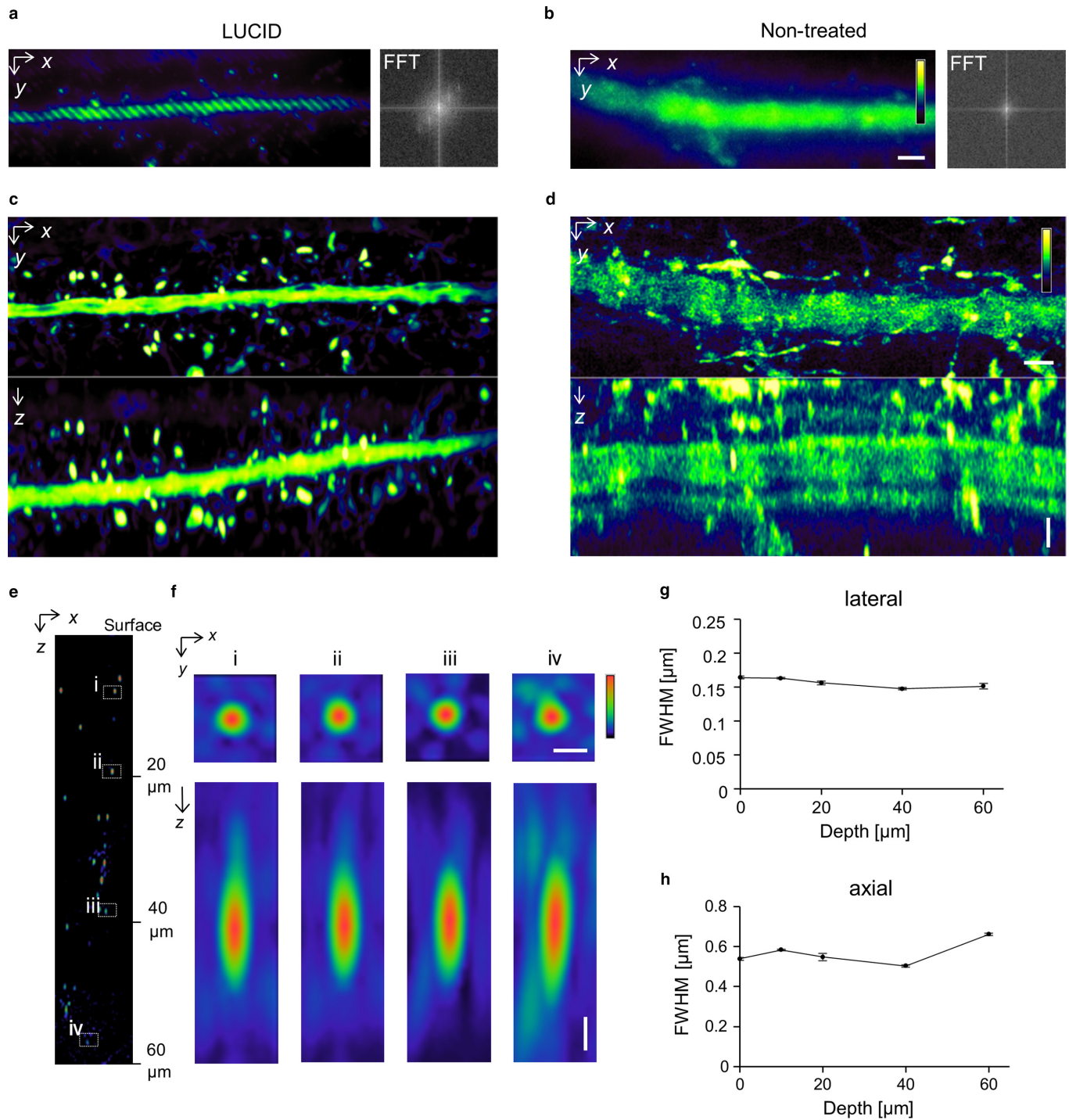


FIG. 3. SIM imaging in LUCID-treated brain slices. (a–d) Representative apical dendrites obtained by super-resolution structured illumination microscopy (SIM) in LUCID- or non-treated brain slices from H-line mice. (a, b) Raw images (left) and frequency spaces of raw images processed by fast Fourier transformation (right) in LUCID- (a) or non- (b) treated slices. (c, d) Reconstructed 3D images of an apical dendrite from raw images acquired in LUCID- (c) or non- (d) treated slices. Scale bars, 2 μm . (e, f) 100-nm YG beads embedded in LUCID-treated slices of wild-type mice. XZ images are shown to a depth of 60 nm from the surface of the slices (e). Fluorescent beads in regions i–iv are shown in XY and XZ images (f). Scale bars, 200 nm. (g, h) Lateral (g) and axial (h) FWHMs of 100-nm YG beads ($n = 10$ each) at each depth. All figures are maximum-intensity projection images. [Colour figure can be viewed at wileyonlinelibrary.com].

(Fig. 4c and e). This potential to visualize accurate forms of spine heads would be advantageous for detecting morphological changes of dendritic spines. Thus, SIM imaging of LUCID-treated slices visualized fine dendritic spines within 200 nm in a broad area of an apical dendrite.

Distribution of spine forms in chronic Dex-treated mice

Next, to demonstrate the potential of SIM imaging, we analyzed spine forms in chronic Dex-treated mice. Chronic treatment with Dex, an agonist of the glucocorticoid receptor, is known to induce

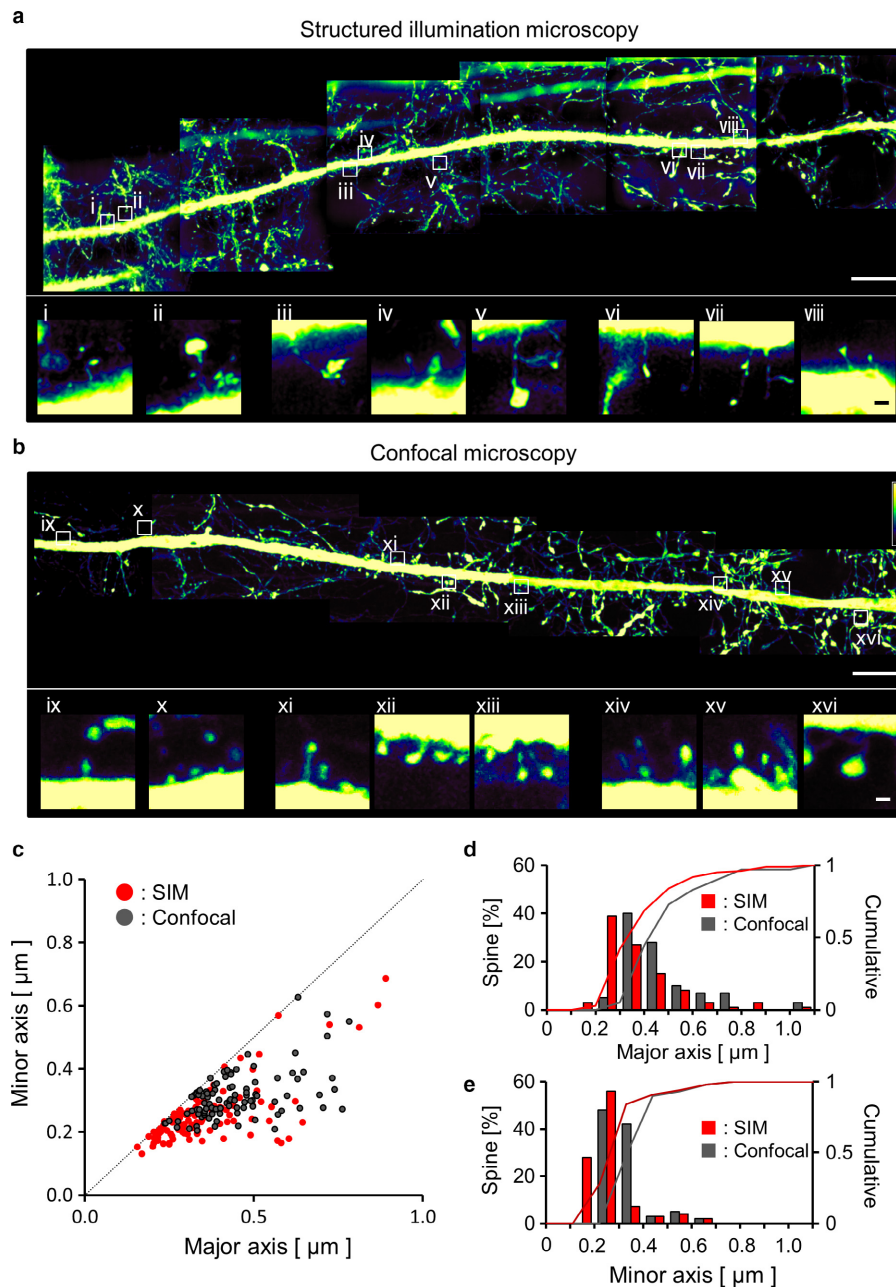


FIG. 4. Dendritic spines on an apical dendrite at L5PNs in SIM and confocal images. (a, b) Representative main shaft of an apical dendrite at L5PNs on the medial prefrontal cortex of H-line mice. The apical dendrite in cortex layers i–v (upper) and dendritic spines of various regions of an apical dendrite (i–xvi) in SIM images (a) and confocal images (b). Scale bars, 10 μm (upper) and 0.5 μm (lower). (c) Scatter plots of spine forms in SIM and confocal images ($n = 100$ each). Spine forms were represented by major and a minor axis of maximum-intensity projection images. (d, e) Percentage of spine numbers as a function of major axis (d) or minor axis (e), shown as histograms with cumulative graphs. All figures were obtained from maximum-intensity projection images. [Colour figure can be viewed at wileyonlinelibrary.com].

depression-like behaviors in rodents (Casarotto & Andreatini, 2007; Sigwalt *et al.*, 2011; Skupio *et al.*, 2015); accordingly, pyramidal neurons in the mPFC are expected to atrophy as in other mouse models of depression (Cerqueira *et al.*, 2007; Banasr *et al.*, 2011; Duman & Duman, 2015). In L5PNs, atrophy has been observed in the tips, but not the main shaft, of apical dendrites. We hypothesized that such atrophy would be detectable by super-resolution microscopy. Thus, we observed the main shaft of the apical dendrite of L5PNs in layers II/III by SIM and confocal microscopy to investigate the effects of chronic Dex treatment (3 weeks; 5 mg/kg; i.p.). Significant shrinkage was not observed in the main shafts of apical

dendrites in chronic Dex-treated mice in comparison with control mice (data not shown). In SIM, the heads of dendritic spines of the Dex-treated group appeared thinner than those in the control group (Fig. 5a and b), although the spine densities did not differ significantly between groups (3.24 ± 1.62 and 3.02 ± 1.51 , respectively). To evaluate forms of spine heads in chronic Dex-treated mice, we tried to represent them as elliptical forms, because the typical classification (Yuste & Bonhoeffer, 2004) was not suitable for morphological analysis of SIM images (See Materials and Methods). To evaluate elliptical forms of dendritic spines, the lengths of the major and minor axes were measured from the maximum-intensity

projection image (Fig. S1b). In the Dex-treated group, spine heads were seemed to be altered to elliptical forms (Fig. 5c). The histogram of the aspect ratio of the spine heads indicated that elliptical spines were more abundant in the Dex-treated group (Fig. 5d). The median values of this ratio in the Dex group and the control group were 1.42 and 1.46 [interquartile range, 1.20–1.67 and 1.24–1.78; $n = 273$ (control), $n = 259$ (Dex) dendritic spines; $n = 3–4$ neurons], respectively. In structural analysis using the aspect ratio, we observed a significant difference between Dex-treated and control mice in SIM images ($Z_{273,259} = -1.962$, $P = 0.04976$), but not in the high-NA confocal images ($Z_{115,221} = 0.61432$, $P = 0.539$; Figs 5e and S4). Thus, SIM imaging showed an altered distribution of spine forms that could not be detected by high-NA confocal imaging.

Discussion

In this study, we demonstrated that 3D-SIM imaging of LUCID-treated brains can visualize dendritic spines along a single dendrite at a spatial resolution of ~ 160 nm. This result suggested that LUCID treatment prevents degradation of focal properties and enables projection of the stripe pattern into deep regions of fixed brains. In addition, this combination revealed an altered distribution of spine forms on the mPFC of chronic Dex-treated mice using a relatively simple method. Thus, this approach represents a high-throughput method for super-resolution analysis of neuronal structures and would be applied to the first screening of abnormal dendritic spines. On the other hand, other super-resolution techniques have also been used to perform such fine structural analysis of neural structures and circuits. For example, stimulated emission depletion microscopy that requires fine adjustment has also achieved super-resolution in single dendrites of fixed brains and acute tissue slices (Bethge *et al.*, 2013; Takasaki *et al.*, 2013; Ke *et al.*, 2016); moreover, in primary neuronal cell cultures, stochastic optical

reconstruction microscopy has been used to study the localization of target molecules bearing blinking fluorescent dyes on synapses (Lakadamyali *et al.*, 2012). By contrast, 3D-SIM only required a striped pattern of excitation laser illumination on the specimen. Thus, 3D-SIM in combination with LUCID treatment should be widely applicable to visualization of neurons expressing conventional fluorescent proteins, even in thick fixed brain slices.

In our evaluation of transparency, we demonstrated that LUCID and TDE60% both induced high transmittance in fixed brains. When using these methods, fluorescence signals are almost completely preserved by immersion in LUCID (data not shown) or low-concentration TDE solution (Aoyagi *et al.*, 2015). In addition, at visible wavelengths, LUCID-treated slices achieved higher transmittance wavelengths than TDE60-treated slices (Fig. 1a–e). This high transparency was probably due to the permeability improved by TDE. These results indicated that LUCID treatment decreases light scattering and the background signal of EYFP. In fluorescence imaging of fixed brains, the imaging volume size was increased in TDE60%- and LUCID-treated slices (Fig. 4a and b). This effect enabled visualization of a large volume of the main shaft of an apical dendrite. In comparison with other recently introduced clearing reagents, LUCID-treated slices were somewhat less transparent, as with TDE-treated slices (Aoyagi *et al.*, 2015). By contrast, LUCID treatment does not require a multistep process (as do ScaleS, SeeDB2 or CLARITY) or long immersion time [as do ScaleS, CLARITY or CUBIC (Clear, Unobstructed Brain Imaging Cocktails and computational analysis)]. Furthermore, LUCID and TDE60% treatment induced almost no destruction of membrane structures, like ScaleS (Fig. 1e), whereas CUBIC, PACT (Passive Clarity Technique) or 3DISCO (3D Imaging of Solvent-Cleared Organs) does induce some damage to membrane structures. Thus, LUCID treatment could be applied to structural analysis of synaptic proteins or the fine forms of dendritic spines in fixed brains.

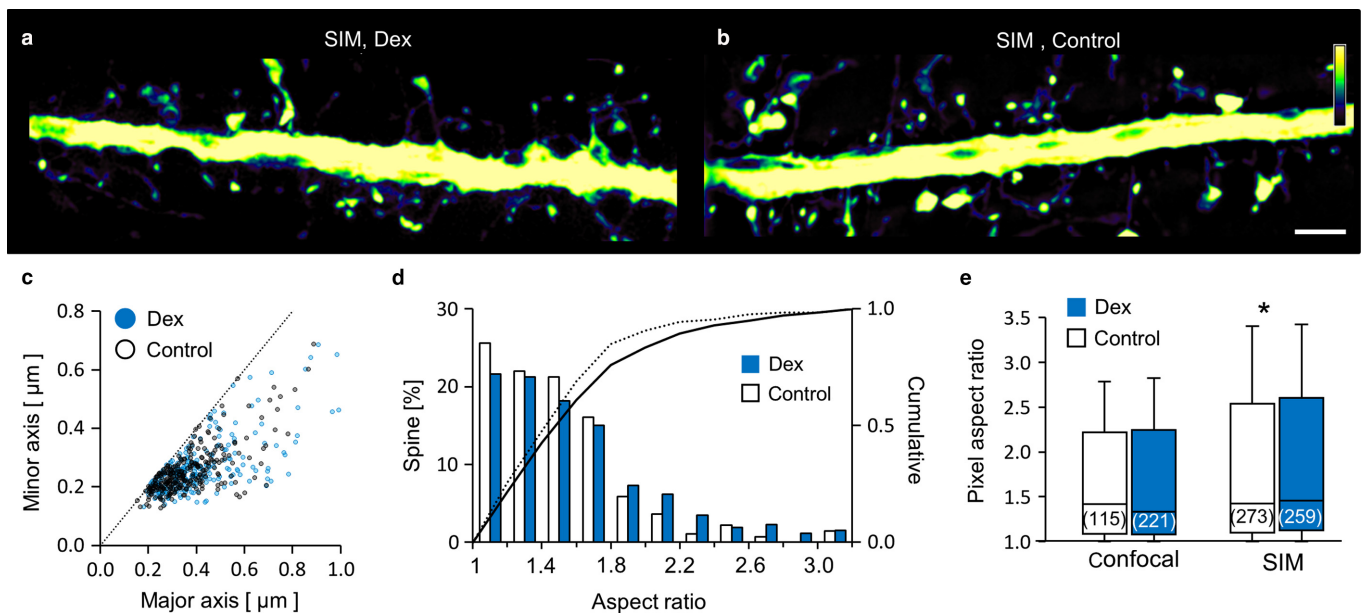


FIG. 5. Distribution of spine forms on L5PNs of mPFC in chronic Dex-treated mice. (a, b) Representative apical dendrites on L5PNs of mPFC in chronic dexamethasone (Dex)-treated (a) or control (b) mice. Scale bars, 2 μ m. (c) Scatter plots of spine forms [$n = 259$ (Dex), $n = 273$ (control)] in Dex-treated or control mice. (d) Percentage of spines vs. aspect ratio, shown as histograms with cumulative curves. The aspect ratio of the spine head was calculated by dividing the major axis by the minor axis. (e) Interquartile range of the aspect ratio of spine heads in Dex-treated or control mice, in comparison with confocal images. Data are shown as interquartile range (Mann–Whitney U -test, $Z_{273,259} = -1.962$, $*P = 0.04976$). All figures were obtained from maximum-intensity projection images. [Colour figure can be viewed at wileyonlinelibrary.com].

LUCID treatment induced improvement of spatial resolution in confocal and 3D-SIM images (Figs 2 and 3). In our confocal images, the remaining optical aberrations (including the spherical aberration) probably deteriorated the FWHMs of fluorescence beads to about 199 nm from the theoretical resolution of 167 nm (NA 1.49; Pawley, 1995). SIM imaging in fixed brains achieved a lateral FWHM of 163 nm and visualized some, although not all, neuronal spine necks. However, in order to reveal spine morphologies including the spine neck, it was necessary to achieve the theoretical resolution of SIM (115 nm). These results indicated that LUCID induced not only high transparency but also reduced spherical aberrations due to the index mismatch, although some optical aberrations persisted in both types of microscopy. In our evaluation of spatial resolution using fluorescence beads, the lateral and axial FWHMs of beads images varied depending on depth and were altered by a correction collar (Fig. S3b and c), which corrected the spherical aberration. Moreover, to correct the remaining optical aberrations, it would be useful to adjust the RI of clearing reagents to 1.515 (Tanabe *et al.*, 2015; Ke *et al.*, 2016). Indeed, we previously proposed adaptive optics containing liquid crystal cells as an alternative approach to reducing various optical aberrations (Tanabe *et al.*, 2015).

In super-resolution imaging of dendritic spines, many spines within 200 nm were visualized in SIM images, but not in high-NA confocal images (Fig. 4c). This result suggested that SIM imaging could be used to reveal altered distributions of spine forms on a single dendrite. To investigate this possibility, we performed structural analysis of spine forms in chronic Dex-treated mice. In our morphological analysis, we focused on apical dendrites in layers II/III, because structural analysis of whole neurons takes a great deal of effort, even in the fluorescence images. SIM images revealed that in the II/III region of chronic Dex-treated mice, the distribution of spine forms on L5PNs of mPFC was altered toward elliptical forms, although no such alterations were detected in high-NA confocal images (Figs 5 and S4). For further detailed analysis of morphologies, it would be necessary to accurately estimate the sizes of dendritic spines from the fluorescence structure or intensity of SIM images. Furthermore, automation of the structural analysis could extend the region of interest in a single neuron. In the future, SIM imaging of all the spines along dendrites could become a useful tool for accurately describing changes of state in neuronal circuits, such as those occurring in psychiatric disease.

Supporting Information

Additional supporting information can be found in the online version of this article:

Fig. S1. The structural analysis of dendritic spines.

Fig. S2. Representative synapses of the striatum region in TDE60% and LUCID-treated brain slices, visualized in transmission electron microscopy.

Fig. S3. 100-nm YG beads images in fixed brain slices, visualized using SIM with various optical conditions.

Fig. S4. Comprehensive analysis of spine forms on L5PNs in confocal images.

Acknowledgements

We thank Dr. K. Otomo, Dr. K. Iijima, and Dr. T. Hibi of the Laboratory of Molecular and Cellular Biophysics at the Research Institute for Electronic Science, Hokkaido University, for helpful advice. We also thank the Nikon Imaging Center at Hokkaido University for technical support. We

are grateful to Vanessa Zheden in the EM facility of IST Austria for technical assistance. This study was supported by MEXT/JSPS KAKENHI grants (No. JP26-1626 to KS; No. JP22113005 to TN and RK; No. JP26242082 to TN and RK; No. JP26650107 to RK; and JP15H05953 'Resonance Bio' to TN and RK) from the Ministry of Education, Culture, Sports, Science and Technology (MEXT) of Japan; by the Nano-Macro Materials, Devices and System Research Alliance (to RK and TN); by the Network Joint Research Center for Materials and Devices (to RK and TN); and in part, by 'Brain Mapping by Integrated Neurotechnologies for Disease Studies (Brain/MINDS)' from the Japan Agency for Medical Research and Development (AMED).

Conflict of interest

The authors declare that there are no competing interests.

Data accessibility

All available data can be obtained by contacting the corresponding author.

Author contributions

K.S., R.K. and T.N. conceived and designed the experiments. K.S. and R.K. performed the SIM and confocal experiments. R.S. performed the electron microscopy experiments. K.S., R.K. and T.N. wrote the manuscript.

Abbreviations

3DISCO, 3D imaging of solvent cleared organs; 3D, three-dimensional; CUBIC, clear, unobstructed brain imaging cocktails and computational analysis; Dex, dexamethasone; EM, electron microscopy; FFT, Fast Fourier Transformation; FWHM, full width at the half maximum; H-line, thy1-EYFP-H transgenic; L5PNs, layer V pyramidal neurons; LUCID, LUCID-A solution; mPFC, medial prefrontal cortex; NA, numerical aperture; PACT, passive clarity technique; SIM, super-resolution structured illumination microscopy; TDE, 2,2'-thiodiethanol; YG, yellow-green.

References

- Aoyagi, Y., Kawakami, R., Osanai, H., Hibi, T. & Nemoto, T. (2015) A rapid optical clearing protocol using 2,2'-thiodiethanol for microscopic observation of fixed mouse brain. *PLoS One*, **10**, e0116280.
- Arellano, J.I., Benavides-Piccione, R., Defelipe, J. & Yuste, R. (2007) Ultrastructure of dendritic spines: correlation between synaptic and spine morphologies. *Front. Neurosci.*, **1**, 131–143.
- Axelrod, D. (2001) Total internal reflection fluorescence microscopy in cell biology. *Traffic*, **2**, 764–774.
- Banasr, M., Dwyer, J. & Duman, R. (2011) Cell atrophy and loss in depression: reversal by antidepressant treatment. *Curr. Opin. Cell Biol.*, **23**, 730–737.
- Bethge, P., Chéreau, R., Avignone, E., Marsicano, G. & Nägerl, U.V. (2013) Two-photon excitation STED microscopy in two colors in acute brain slices. *Biophys. J.*, **104**, 778–785.
- Booth, M., Neil, M. & Wilson, T. (1998) Aberration correction for confocal imaging in refractive-index-mismatched media. *J. Microsc.-Oxford*, **192**, 90–98.
- Casarotto, P. & Andreatini, R. (2007) Repeated paroxetine treatment reverses anhedonia induced in rats by chronic mild stress or dexamethasone. *Eur. Neuropsychopharm.*, **17**, 735–742.
- Cerqueira, J., Taipa, R., Uylings, H., Almeida, O. & Sousa, N. (2007) Specific configuration of dendritic degeneration in pyramidal neurons of the medial prefrontal cortex induced by differing corticosteroid regimens. *Cereb. Cortex*, **17**, 1998–2006.
- Collin, C., Miyaguchi, K. & Segal, M. (1997) Dendritic spine density and LTP induction in cultured hippocampal slices. *J. Neurophysiol.*, **77**, 1614–1623.
- Conchello, J.A., Kim, J.J. & Hansen, E.W. (1994) Enhanced three-dimensional reconstruction from confocal scanning microscope images. II. Depth discrimination versus signal-to-noise ratio in partially confocal images. *Appl. Optics*, **33**, 3740–3750.
- Cox, G. & Sheppard, C. (2004) Practical limits of resolution in confocal and non-linear microscopy. *Microsc. Res. Techniq.*, **63**, 18–22.

- Duman, C. & Duman, R. (2015) Spine synapse remodeling in the pathophysiology and treatment of depression. *Neurosci. Lett.*, **601**, 20–29.
- Feng, G., Mellor, R.H., Bernstein, M., Keller-Peck, C., Nguyen, Q.T., Wallace, M., Nerbonne, J.M., Lichtman, J.W. *et al.* (2000) Imaging neuronal subsets in transgenic mice expressing multiple spectral variants of GFP. *Neuron*, **28**, 41–51.
- Gibson, S. & Lanni, F. (1991) Experimental test of an analytical model of aberration in an oil-immersion objective lens used in 3-dimensional light-microscopy. *J. Opt. Soc. Am. A*, **8**, 1601–1613.
- Gustafsson, M.G. (2000) Surpassing the lateral resolution limit by a factor of two using structured illumination microscopy. *J. Microsc.-Oxford*, **198**, 82–87.
- Hama, H., Kurokawa, H., Kawano, H., Ando, R., Shimogori, T., Noda, H., Fukami, K., Sakaue-Sawano, A. *et al.* (2011) Scale: a chemical approach for fluorescence imaging and reconstruction of transparent mouse brain. *Nat. Neurosci.*, **14**, 1481–1488.
- Hama, H., Hioki, H., Namiki, K., Hoshida, T., Kurokawa, H., Ishidate, F., Kaneko, T., Akagi, T. *et al.* (2015) ScaleS: an optical clearing palette for biological imaging. *Nat. Neurosci.*, **18**, 1518–1529.
- Harris, K.D. & Shepherd, G.M. (2015) The neocortical circuit: themes and variations. *Nat. Neurosci.*, **18**, 170–181.
- Kasthuri, N. & Lichtman, J.W. (2003) The role of neuronal identity in synaptic competition. *Nature*, **424**, 426–430.
- Ke, M.T., Nakai, Y., Fujimoto, S., Takayama, R., Yoshida, S., Kitajima, T.S., Sato, M. & Imai, T. (2016) Super-resolution mapping of neuronal circuitry with an index-optimized clearing agent. *Cell Rep.*, **14**, 2718–2732.
- Kim, A. & Wilson, B.C. (2011) Measurement of *ex vivo* and *in vivo* tissue optical properties: methods and theories. In Welch, A.J. & Gemert, M.J.C.V. (Eds), *Optical-Thermal Response of Laser-Irradiated Tissues*. Springer, Dordrecht, The Netherlands, pp. 267–319.
- Lakadamyali, M., Babcock, H., Bates, M., Zhuang, X. & Lichtman, J. (2012) 3D multicolor super-resolution imaging offers improved accuracy in neuron tracing. *PLoS One*, **7**, e30826.
- Lichtman, J.W., Livet, J. & Sanes, J.R. (2008) A technicolour approach to the connectome. *Nat. Rev. Neurosci.*, **9**, 417–422.
- Livet, J., Weissman, T.A., Kang, H., Draft, R.W., Lu, J., Bennis, R.A., Sanes, J.R. & Lichtman, J.W. (2007) Transgenic strategies for combinatorial expression of fluorescent proteins in the nervous system. *Nature*, **450**, 56–62.
- Matsuzaki, M., Ellis-Davies, G.C., Nemoto, T., Miyashita, Y., Iino, M. & Kasai, H. (2001) Dendritic spine geometry is critical for AMPA receptor expression in hippocampal CA1 pyramidal neurons. *Nat. Neurosci.*, **4**, 1086–1092.
- Mizutani, H., Ono, S., Ushiku, T., Kudo, Y., Ikemura, M., Kageyama, N., Yamamichi, N., Fujishiro, M. *et al.* (2018) Transparency-enhancing technology allows three-dimensional assessment of gastrointestinal mucosa: a porcine model. *Pathol. Int.*, **68**, 102–108.
- Neil, M.A., Juskaitis, R. & Wilson, T. (1997) Method of obtaining optical sectioning by using structured light in a conventional microscope. *Opt. Lett.*, **22**, 1905–1907.
- Nusser, Z., Lujan, R., Laube, G., Roberts, J.D., Molnar, E. & Somogyi, P. (1998) Cell type and pathway dependence of synaptic AMPA receptor number and variability in the hippocampus. *Neuron*, **21**, 545–559.
- Onodera, H. (2014) Method for rendering tissue transparent, reagent for rendering tissue transparent, and tissue observation method. Google Patents.
- Pawley, J.B. (1995) *Handbook of Biological Confocal Microscopy*. Plenum Press, New York, NY.
- Richardson, D.S. & Lichtman, J.W. (2015) Clarifying tissue clearing. *Cell*, **162**, 246–257.
- Sheppard, C., Gu, M., Brain, K. & Zhou, H. (1994) Influence of spherical-aberration on axial imaging of confocal reflection microscopy. *Appl. Optics*, **33**, 616–624.
- Shigematsu, N., Ueta, Y., Mohamed, A.A., Hatada, S., Fukuda, T., Kubota, Y. & Kawaguchi, Y. (2016) Selective thalamic innervation of rat frontal cortical neurons. *Cereb. Cortex*, **26**, 2689–2704.
- Sigwalt, A., Budde, H., Helmich, I., Glaser, V., Ghisoni, K., Lanza, S., Cadore, E., Lhullier, F. *et al.* (2011) Molecular aspects involved in swimming exercise training reducing anhedonia in a rat model of depression. *Neuroscience*, **192**, 661–674.
- Skupio, U., Tertilt, M., Sikora, M., Golda, S., Wawrzczak-Bargiela, A. & Przewlocki, R. (2015) Behavioral and molecular alterations in mice resulting from chronic treatment with dexamethasone: relevance to depression. *Neuroscience*, **286**, 141–150.
- Takasaki, K.T., Ding, J.B. & Sabatini, B.L. (2013) Live-cell superresolution imaging by pulsed STED two-photon excitation microscopy. *Biophys. J.*, **104**, 770–777.
- Tanabe, A., Hibi, T., Ipponjima, S., Matsumoto, K., Yokoyama, M., Kurihara, M., Hashimoto, N. & Nemoto, T. (2015) Correcting spherical aberrations in a biospecimen using a transmissive liquid crystal device in two-photon excitation laser scanning microscopy. *J. Biomed. Opt.*, **20**, 101204.
- Tønnesen, J. & Nägerl, U.V. (2013) Superresolution imaging for neuroscience. *Exp. Neurol.*, **242**, 33–40.
- Tønnesen, J., Katona, G., Rózsa, B. & Nägerl, U.V. (2014) Spine neck plasticity regulates compartmentalization of synapses. *Nat. Neurosci.*, **17**, 678–685.
- Urban, N.T., Willig, K.I., Hell, S.W. & Nägerl, U.V. (2011) STED nanoscopy of actin dynamics in synapses deep inside living brain slices. *Biophys. J.*, **101**, 1277–1284.
- Yuste, R. & Bonhoeffer, T. (2004) Genesis of dendritic spines: insights from ultrastructural and imaging studies. *Nat. Rev. Neurosci.*, **5**, 24–34.